Space Weather®

RESEARCH ARTICLE
10.1029/2022SW003111

Large Geomagnetically Induced Currents at Equator Caused by an Interplanetary Magnetic Cloud

B. Nilam[1] and **S. Tulasi Ram**[1]

[1]Indian Institute of Geomagnetism, Navi Mumbai, India

Key Points:

- Unique report of large d*B*/d*t* (geomagnetically induced current) at the geomagnetic equator due to a decrease in solar wind density at the front boundary of a magnetic cloud
- The amplitude of d*B*/d*t* is maximized at the equator on the noon side due to the Equatorial ElectroJet and is compared to that at high latitudes
- Solar wind density takes the control of dayside reconnection and convection electric fields through the modulation of magnetosheath Bz

Correspondence to:
B. Nilam,
nilambhosale0@gmail.com

Citation:
Nilam, B., & Tulasi Ram, S. (2022). Large geomagnetically induced currents at equator caused by an interplanetary magnetic cloud. *Space Weather*, *20*, e2022SW003111. https://doi.org/10.1029/2022SW003111

Received 31 MAR 2022
Accepted 10 MAY 2022

Abstract Here, we report a rare observation of an extremely large and rapid change of geomagnetic field (d*B*/d*t*), a proxy for the geomagnetically induced currents (GICs), at the equator caused by a sudden drop in solar wind density at the front boundary of a magnetic cloud (MC) during the great 31 March 2001 storm. The horizontal component at the Indian equatorial station, Tirunelveli, recorded a sharp decline of ∼350 nT in just 5 min with a peak d*B*/d*t* exhibiting a concerning value of 136 nT/min, a possible GIC risk to the electric power systems. The responsible physical mechanisms were examined through magneto-hydrodynamic model simulations and found that a prompt penetration of strong westward-overshielding electric fields and ionospheric currents at the equator play a dominant role. This study provides some new insights into the extent of extreme geomagnetic field changes that can occur at the equatorial region due to solar wind density reduction at MC, which can have potential impacts on the electric power grid systems.

Plain Language Summary The Earth, a planet with an intrinsic magnetic field bubble around it, is immersed in a hot and energetic solar wind plasma that continuously emanated from the Sun. The sudden disturbances on the Sun, such as coronal mass ejections, induce transient structures in the solar wind which, when directed earthward, can cause severe disturbances in the Earth's (Geo) magnetic field. The rapid changes in the geomagnetic field induce electric fields at the conducting surface of Earth, which can cause strong electrical currents, known as geomagnetically induced currents (GICs), that flow through the long conducting structures, like electric power transmission lines, long pipelines, etc., on the ground. The enhanced GICs are of serious threat to the electric power and pipeline grids. The elevated GICs are most popularly known to occur at high latitudes during severe geomagnetic storms. This study reports a rare observation of a large and rapid change in geomagnetic field indicating the strong GICs at the geomagnetic equator due to a magnetic cloud structure in solar wind and reveals the underlying physical processes.

1. Introduction

Transient structures in the solar wind can induce significant disturbances in the Earth's magnetosphere-ionosphere system. Coronal mass ejections (CMEs), the large-scale magnetic structures emanated from the Sun, are of particular importance given their geo-effectiveness and have been studied in great detail (Balan et al., 2017; Cliver et al., 2003; Gopalswamy, 2003, 2006; Gosling et al., 1996 and references therein). Due to their high speeds, CMEs drive shocks on their transit through the interplanetary (IP) space. A typical IP CME structure consists of a forward shock, a magnetic cloud (MC), and a shock-sheath region sandwiched between the two (Burlaga et al., 1981, 1982, 1998; Gopalswamy, 2006; Lepping et al., 1990, 1997; Wang et al., 2003). The forward shock of a CME is typically characterized by a sudden enhancement in the solar wind velocity, temperature, density, and magnetic field measured by spacecraft at L1-point. Due to the enhanced solar wind dynamic pressure, the forward shocks of CMEs when impinging on the Earth's magnetosphere transfer momentum and energy leading to a significant compression of Earth's magnetosphere and enhanced magnetopause currents (Araki, 1977, 1994; Ober et al., 2002; Russell, 1976). The geomagnetic field manifestations of IP shocks mainly comprise storm sudden commencements (SCs) and sudden impulses (SIs; Araki, 1977; Takeuchi et al., 2002). The SCs are characterized by a sudden enhancement in the geomagnetic field followed by a geomagnetic storm, whereas the SIs have a sharp increase (SI^+) or decrease (SI^-) in the geomagnetic field for a short duration (few minutes) and can occur during the storm or even outside the interval of a storm period (during quiet period; Carter et al., 2015; Nilam et al., 2020; Sastri, 2002; Sastri et al., 1995; Tulasi Ram et al., 2019). The rapid changes in the geomagnetic field during SCs and SIs can generate the geomagnetically induced currents (GICs) on the ground and can cause potential damages to electric power grids and long transmission lines (Baker, 2002; Carter et al., 2015; Oliveira et al., 2018; Pulkkinen et al., 2012; Takeuchi et al., 2002; Viljanen, 1998). The amplitude

of GICs is often represented by the rate of change of the geomagnetic field (dB/dt) on the ground. Generally, a typical value of 100 nT/min for dB/dt is considered to be the concerning value for the GIC risk on electrical power systems (Carter et al., 2015; Gaunt & Coetzee, 2007; Kappenman, 2005; Oliveira et al., 2018). The large values of dB/dt are usually observed at high latitudes due to the presence of strong auroral electrojet currents. Accordingly, the majority of the earlier studies on the SI and GIC impacts were focused at high latitudes, but the impacts of SIs on equatorial GICs have received relatively less attention.

Several studies have shown that the sudden geomagnetic field disturbances (SIs) are significant at equatorial latitudes although they are usually weaker compared to that at auroral latitudes (Nilam et al., 2020; Sastri, 2002; Sastri et al., 1995; Tulasi Ram et al., 2019). A strong jet of ionospheric current flows in the narrow band (±2°) of latitudes centered on the geomagnetic equator due to the enhanced Cowling conductivity known as an "Equatorial Electrojet." During day time, this current flows in the eastward direction in the E-region of the equatorial ionosphere and maximizes around local noon (Kane, 1974; Rastogi, 1977; Reddy, 1989). Recent studies by Carter et al. (2015, 2016) have shown the severalfold amplifications of SIs at equatorial latitudes due to the equatorial electrojet during the fast IP shocks. Oliveira et al. (2018) have studied 547 IP shocks during two solar cycles (1995–2017) and found that the large dB/dt cases were generally associated with high-speed and nearly frontal IP shocks. They have identified nine equatorial GIC events with the $dB/dt > 100$ nT/min and were all associated with high-speed forward shocks of CMEs, impinging the magnetosphere at a low impact angles. All the nine events were SCs followed by the geomagnetic storms. The studies of Carter et al. (2015, 2016) and Oliveira et al. (2018) suggest the importance of high-speed CME forward shocks and their impact angles for the large dB/dt at equatorial latitudes. These aspects facilitate the forecast of risk alerts to the power system operators based on the upstream solar wind parameters in ∼30–60 min advance (Oliveira et al., 2018).

In this paper, we present a unique observation of a large negative SI (SI^-) at the equator in response to a sudden drop in solar wind density at the front boundary of a MC during an intense geomagnetic storm on 31 March 2001. This SI^- exhibited a dB/dt value of 136 and 19.1 nT at 1-min and 5-s scales, respectively, at the equator in response to a sudden decrease of solar wind density by ∼16 particles/cm^3. Such an extremely large negative SI at the equatorial station is very rare. Therefore, understanding the physical mechanisms responsible for such a large negative SI is very important for GIC risk forecasters. Our study emphasizes the extent of SI^- that can occur at equatorial latitudes during MC and unveils the responsible physical mechanisms through magneto-hydro-dynamic (MHD) model simulations.

2. Data

A total of 86 ground-based magnetometer observations from INTERMAGNET (https://www.intermagnet.org/) and World Data Center for Geomagnetism (http://wdc.kugi.kyoto-u.ac.jp/), the Kyoto University were considered to study the geomagnetic field variations during the 31 March 2001 storm. The solar wind parameters observed by the ACE spacecraft (time shifted to bow-shock nose) and SymH index data at 1-min resolution were obtained from the NASA OMNI-Space Physics Data Facility (https://omniweb.gsfc.nasa.gov/). Further, a pair of magnetometer observations from the Indian equatorial station, Tirunelveli (Geog. Lat 8.7°N and Geog. Long 77.81°E), and low-latitude station, Alibag (Geog. Lat 18.64°N and Geog. Long 72.87°E), were analyzed. The geomagnetic latitudes of Tirunelveli and Alibag (computed using the quasi-dipole-based coordinate system and coefficients of all-spherical harmonic degrees of International Geomagnetic Reference Field for the epoch 31 March 2001) are 0.34°S and 10.03°N, respectively. The ΔH values at Tirunelveli (ΔH_{TIR}) and Alibag (ΔH_{ABG}) are computed by subtracting the internal field and solar quiet current contributions (average diurnal variation of five international quiet days in that month) for comparison with Sym-H. The magnetometer observations at Tirunelveli are available at 1-min and 5-s time resolutions, whereas the magnetometer observations at Alibag are available at 1-min resolution.

3. Results

Figure 1 shows the UT variations of solar wind parameters (IMF B, Bz, velocity, temperature, density, and dynamic pressure) and ground observations, such as, SymH, ΔH_{TIR}, and ΔH_{ABG}, during 31 March 2001. The arrival of CME forward shock can be noted in solar wind parameters around 0114 UT (Figures 1a–1e) and the occurrence of SC can be seen in SymH, ΔH_{TIR}, and ΔH_{ABG} (Figure 1f). The main phase of the storm has started

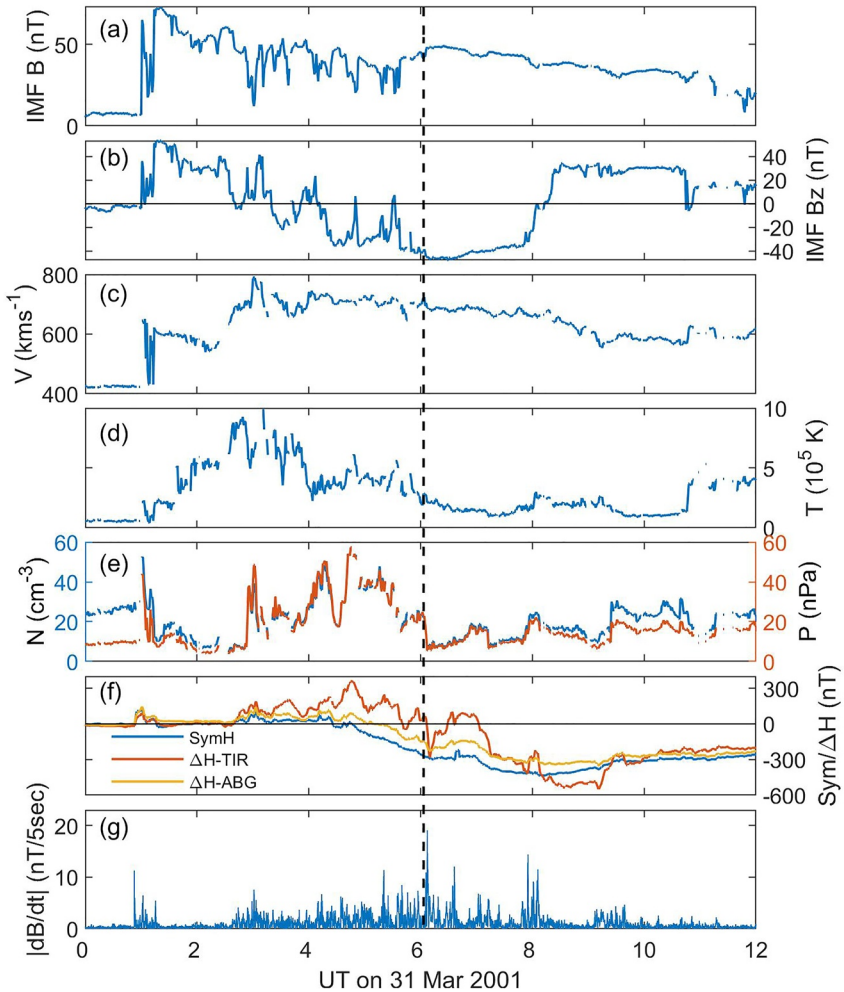

Figure 1. Universal time variations of upstream solar wind parameters, (a) IMF B; (b) IMF Bz; (c) velocity; (d) temperature; (e) density, pressure, and ground geomagnetic field variations; (f) SymH, ΔH_{TIR}, ΔH_{ABG}; and (g) $|dB/dt|$ at Tirunelveli during the great geomagnetic storm of 31 March 2001. The black vertical dashed line indicates the time of sharp density reduction at the front boundary of a magnetic cloud.

around ~0410 UT with the southward turning of IMF Bz. Both the SymH and ΔH_{ABG} are steadily decreasing, however, with a positive offset in the ΔH_{ABG} (in the morning to noon sector) compared to the longitudinally averaged SymH. In contrast, the equatorial ΔH_{TIR} exhibits positive values till 0600 UT and more or less mimics the variations in solar wind density and/or dynamic pressure. The event of interest here, a sudden decrease in density by about 16 particles/cm^3 (Figure 1e), occurred during 0605–0610 UT (marked by a black vertical line). This drop in density is associated with the front boundary of the MC as one can see the clear MC signatures, like enhanced B (Figure 1a), smooth rotation of Bz (Figure 1b), steady decrease of velocity (Figure 1c), low temperatures (Figure 1d), and sharp decrease in density (Figure 1e) (Burlaga et al., 1981; Klein & Burlaga, 1982; Wang et al., 2003). In response to this drop in density, the ΔH_{TIR} (Figure 1f) exhibited a sharp decrease of ~350 nT (in just 5 min). On the other hand, the low latitude ΔH_{ABG} (Figure 1f) exhibited only a small decrease of ~82 nT over the same longitude/local time sector during this period. Figure 1g shows the variation of $|dB/dt|$ at Tirunelveli derived at 5-s resolution. Please note that the B in this study is the same horizontal component of geomagnetic field ($B = B_H = \sqrt{B_x^2 + B_y^2}$), where B_x and B_y are the northward and eastward components, respectively. One can observe that the $|dB/dt|$ at Tirunelveli exhibits a large value of 19.1 nT/5 s at 0608 UT, which is very unusual for a location outside the auroral region. The corresponding change at 1-min time resolution is 136 nT/min.

Further, with a view to compare the dB/dt at Tirunelveli with other locations over the globe, the magnetometer observations from 86 INTERMAGET stations were analyzed for dB/dt at different locations as shown in Figure 2.

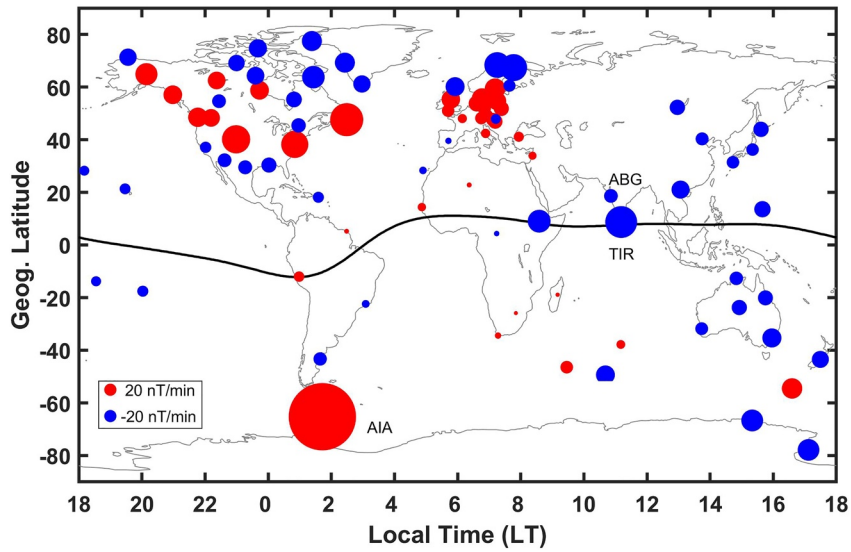

Figure 2. Peak dB/dt observed during the period 0605-0610 from 86 magnetometer stations across the globe. The size of the circle represents the magnitude of SI; the red and blue colors represent the SI^+ and SI^-, respectively. The black curve represents the geomagnetic equator. The x axis shown in local time corresponds to 0608 UT.

Here, the dB/dt at all the locations are computed at 1-min time resolution for comparison. The red and blue color circles represent the positive and negative changes (SI^+ and SI^-), respectively, and the size of circles indicates the magnitude of dB/dt. The black curve represents the geomagnetic equator and the x axis is shown in local time corresponding to this event (0608 UT). The dB/dt is mostly positive at auroral latitudes (over northern USA, Canada, and Europe) on the nightside and mostly negative above and below the auroral region. Interestingly, the dB/dt at Tirunelveli is the largest value (−136 nT/min) compared to all other available locations barring a southern high-latitude station, Argentine Island (AIA), where the dB/dt is ∼600 nT/min. The large dB/dt at AIA could be due to strong auroral currents in the midnight sector; however, further discussion on changes at AIA is beyond the scope of this paper. Further, it is interesting to note that the dB/dt values in the close vicinity of geomagnetic equator (the black curve) are clearly negative on the dayside and slightly positive on the night side. Also, the magnitude of dB/dt is maximized at Tirunelveli around the noon sector compared to other sectors. On the other hand, the dB/dt at the low-latitude station Alibag (about 10° away from the equator) is significantly smaller (−25 nT/min) over the same local time sector. These results clearly indicate that the amplitude of SI^- in response to a sudden density drop at MC is significantly enhanced at equatorial latitudes of noon sector and is comparable or even higher than that at high latitudes.

4. Discussion

A sudden decrease in the solar wind density and/or withdrawal of dynamic pressure causes rapid relaxation of magnetosphere from a previously compressed state and retreat of magnetopause currents. These changes in the magnetosphere manifest as a geomagnetic SI^- at low to midlatitudes. Interestingly, the dB/dt at the equator is −136 nT/min, which is more than five times larger compared to dB/dt of −25 nT/min at Alibag (Figure 2). However, the effects of magnetosphere expansion and the reduction in magnetopause current do not expected to exhibit such a large difference between the two stations separated by about ∼10° apart. This clearly indicates the dominant role of equatorial ionospheric currents contributing for the observed difference between the two stations.

Further, with a view to compare the observed changes at Tirunelveli and Alibag with the global-scale low-latitude ring current index SYM-H, we have calculated the ratios of dB/dt to d(Sym-H)/dt for these two stations as shown in Figure 3. One can clearly see from this figure that the dB/dt is significantly amplified (78 times) with respect to d(Sym-H)/dt at Tirunelveli compared to that at Alibag (∼25 times) in response to the sudden drop in the solar wind density (black vertical dashed line) at 0608 UT. Therefore, this large equatorial enhancement in dB/dt observed at Tirunelveli can be primarily attributed to the change in EEJ in response to the sudden decrease

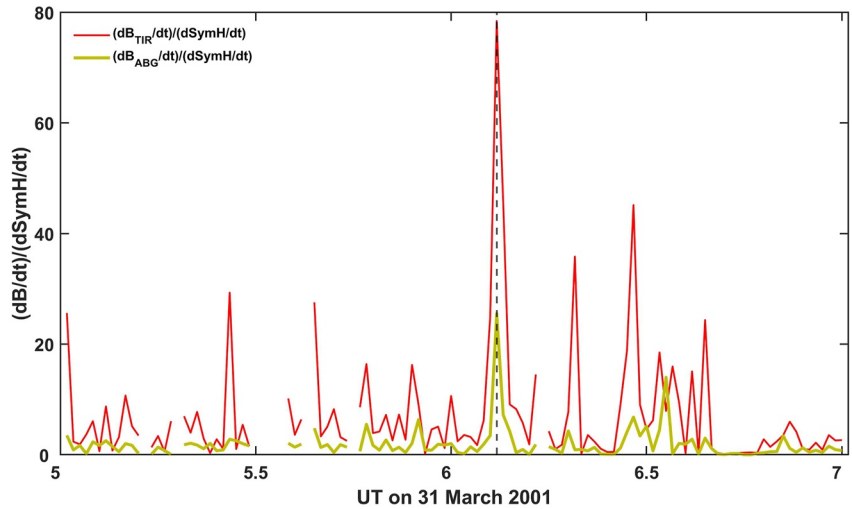

Figure 3. UT variation of d*B*/d*t* to d(Sym-H)/d*t* ratios at Alibag and Tirunelveli stations.

in solar wind density. Carter et al. (2015) and Oliveira et al. (2018) also have shown that the magnitude of SI is amplified several times at the equator due to the equatorial electrojet and maximizes around noon time.

Now, we focus our investigation on the physical mechanisms responsible for the observed changes in the EEJ in response to the density drop at MC. For this purpose, we performed the MHD model simulations using the Block-Adaptive-Tree-SolarWind-Roe-Upwind-Scheme (BATSRUS) model coupled with the Ring Current Model (RCM) under the Space Weather Modeling Framework (SWMF; Liemohn et al., 2018; Ridley & Liemohn, 2002; Tóth et al., 2005). The RCM modifies the plasma pressure distribution in the inner magnetosphere and changes the resulting field-aligned currents in the ionosphere and thus yields more realistic Region-1 and Region-2 currents when coupled with the BATSRUS model (Harel et al., 1981; Liemohn et al., 2018; Toffoletto et al., 2003). The BATSRUS model also couples with the Ridley Ionosphere Model (RIM) to solve the ionospheric electrodynamics (Haiducek et al., 2017; Morley et al., 2018; Pulkkinen et al., 2013; Ridley, 2004). The BATSRUS model simulations are carried out with the OMNI time-shifted solar wind inputs on the Community Coordinated Modeling Center (CCMC) platform and the results are presented in Figure 4. Figures 4a and 4b shows the Bz variation in the GSM-*XY* plane at 0604 and 0608 UT, respectively. One can observe that the magnetosphere is highly compressed with magnetopause that is below 6 Re (Earth radii) and bow shock is around 10 Re at 0604 UT due to strong dynamic pressure by the shock-sheath region of ICME. The Bz in the magnetosheath region is strongly southward (∼−150 nT) due to strong compression in the magnetosheath region. At 0608 UT, the magnetopause is expanded to >6.5 Re and the bow shock is swiftly shifted to nearly 20 Re in response to a sudden decrease in density at the front boundary of MC. In fact, the dayside magnetosphere is not expanded significantly (magnetopause is shifted by only ∼0.5–1 Re); however, the magnetosheath region exhibited a dramatic expansion of nearly 10 Re from a highly compressed state prior to the MC. As a result, the Bz flux density in the magnetosheath region is reduced significantly as can be seen from the figure.

It is well known that the transfer of solar wind energy into the Earth's magnetosphere–ionosphere system is largely controlled by the southward IMF Bz through the dayside magnetic reconnection. In fact, the Bz in the magnetosheath region actually determines the reconnection rate at magnetopause and the energy transfer to the magnetosphere (Kataoka et al., 2005). To closely observe the variations of Bz near the dayside reconnection (magnetopause) region, the variations of Bz at 6–7 Re from the MHD simulation are plotted in Figure 4d. The corresponding variations of upstream solar wind density (blue curve), velocity (green curve), and IMF Bz (red curve) are shown in Figure 4c. One can see that both the solar wind velocity and IMF Bz are more or less steady at 700 km/s and −40 nT, respectively, throughout this period. The Bz at 6–7 Re is strongly southward till 0604 UT (prior to the MC), representing the magnetosheath region and indicating that the magnetopause is pushed below 6 Re due to strong compression. Ober et al. (2002) have also shown that the magnetosphere is highly compressed and the magnetopause is under the geosynchronous orbit during this storm period using satellite observations (Figure 3 of Ober et al., 2002). With the sudden decrease in density at 0605 UT, the Bz at 6–6.5 Re

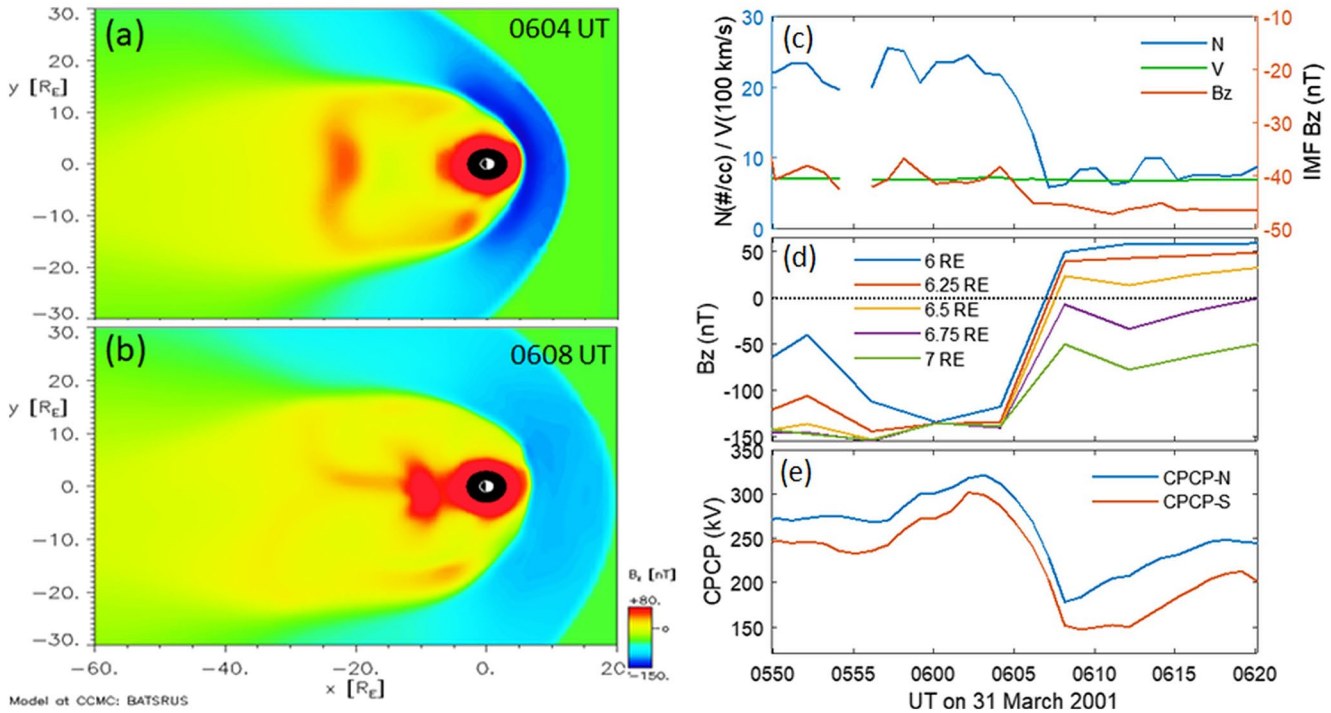

Figure 4. Results of magneto-hydro-dynamic (MHD) simulation using the Block-Adaptive-Tree-SolarWind-Roe-Upwind-Scheme model coupled with the Ring Current Model. Panels (a) and (b) show the variation of Bz in the GSM-*XY* plane during 0604 and 0608 UT, respectively. (c) Variations of upstream solar wind velocity (green), density (blue), and IMF BZ measured at L1-point. (d) Bz variations at 6–7 Re from the MHD simulation. (e) Cross polar cap potential (CPCP) variations at Northern and Southern Hemispheres as a function of UT.

sharply reverses to northward. The northward Bz at 6–6.5 Re represents the geomagnetic field, indicating that the magnetopause is retraced to >6.5 Re in response to the density decrease at MC. The Bz at 6.75 Re (and 7 Re) also sharply recovered from −140 to −7 nT (and −50 nT) but remains southward. This indicates that the magnetopause where the dayside magnetic reconnection occurs is shifted to a location between 6.5 and 6.75 Re. Note that even the upstream IMF Bz is more or less steady (with a small increase in southward direction, Figure 4c), the magnetosheath Bz field at 6.75 Re has reduced by nearly 20 times due to the decrease in density (Figure 4d). This decrease in magnetosheath Bz field reduces the dayside reconnection rate at magnetopause and causes a sharp reduction in the high-latitude convection. Figure 4e shows the sharp reduction of cross polar cap potential at both Northern (CPCP-N) and Southern (CPCP-S) Hemispheres. This clearly indicates that the dayside reconnection rate and the high-latitude convection electric fields are sharply reduced with the decreased density at the front boundary of MC. Lopez et al. (2004) and Kataoka et al. (2005) have also shown that the steady and strong southward Bz conditions during geomagnetic storms can lower down the Mach number to a level where the solar wind density takes the control of the dayside reconnection rate and polar cap potential. Ober et al. (2007) have shown that the decrease of CPCP is caused by the decrease in the dayside reconnection rate to accommodate the needed accumulation of closed magnetic flux during the fast rarefaction wave driven by the sudden decrease in density. The decrease in the reconnection rate causes a sharp reduction in the high-latitude convection electric field and leads to a situation where the shielding electric field dominates, known as the overshielding condition (Kikuchi et al., 1996, 2003). The convection and shielding electric fields communicate with the high-latitude ionosphere via region-1 and region-2 field-aligned currents, respectively (Nishida, 1968; Senior & Blanc, 1984). Figure 5 shows the region-1 and region-2 field-aligned currents from the MHD simulation. The strong region-1 currents (flows inward at dawn and outward at dusk) prevailing during 0604 UT (prior to the MC) were reduced and the region-2 currents (flows inward at dusk and outward from dawn) become dominant at 0612 UT with the decrease in density at MC. The dominant region-2 currents indicate the strong westward-shielding electric fields, which penetrate promptly to the low latitudes via TM0 mode propagation through the Earth-ionosphere waveguide (Kikuchi et al., 1996, 2003). The westward prompt penetration electric fields (PPEF) cause a sharp negative perturbation in the equatorial B-field due to the enhanced Cowling conductivity and the equatorial electrojet.

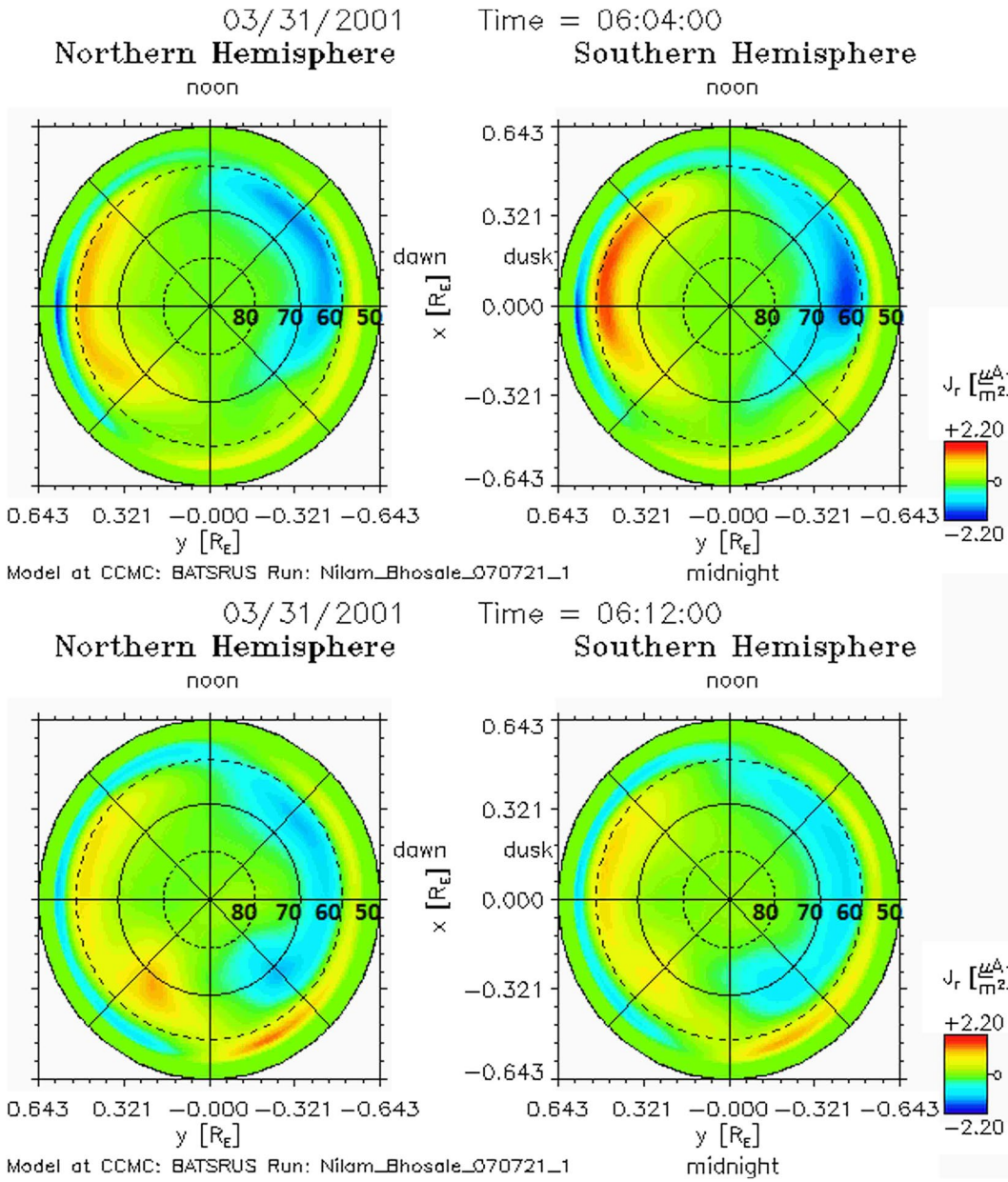

Figure 5. Radial currents from magneto-hydro-dynamic simulations using the Block-Adaptive-Tree-SolarWind-Roe-Upwind-Scheme model coupled with the Ring Current Model representing the Region-1 and Region-2 currents at Northern (left panels) and Southern (right panels) Hemispheres (poleward of 50°) during 0604 UT (top panels) and 0612 UT (bottom panels).

Therefore, the large SI^- observed at Tirunelveli is mainly due to the strong westward PPEF in response to sharp reduction in the solar wind density at MC through a sudden reduction in convection electric fields (dominance of shield fields) via a reduction in the dayside reconnection rate.

The MHD model used in this study also provides the simulated ground dB/dt values at the selected locations under the SWMF. For this purpose, the model computes the sum of magnetic field perturbations originating from the magnetosphere, contributions from field-aligned currents, and the contributions from the Hall and Pederson currents in the ionosphere using the Biot-Savart technique (Kwagala et al., 2020; Yu & Ridley, 2008). It uses the RIM to solve the ionospheric electrodynamics, and the ionospheric conductance is calculated by taking the solar irradiance and field-aligned current from the BATSRUS model (Haiducek et al., 2017; Morley et al., 2018;

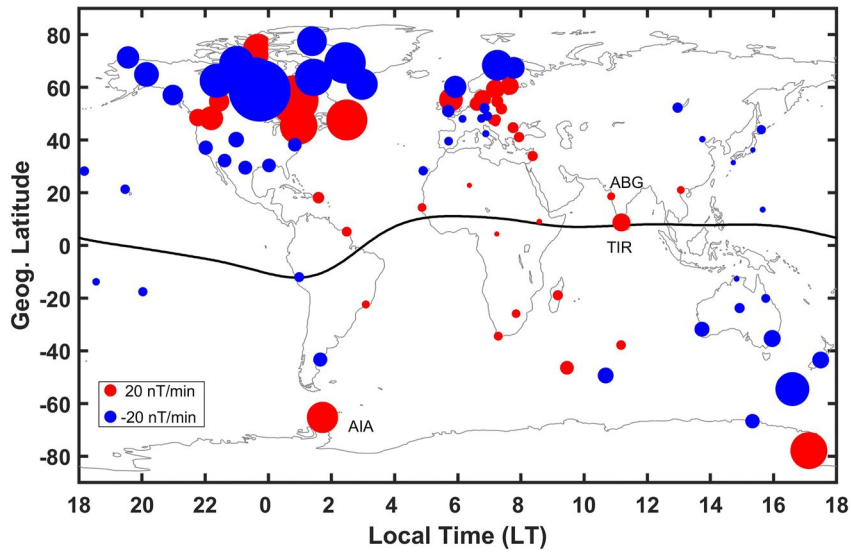

Figure 6. Same as Figure 2, except that the d*B*/d*t* values are computed by the magneto-hydro-dynamic model.

Pulkkinen et al., 2013; Ridley, 2004). Figure 6 shows the peak d*B*/d*t* values between 0605 and 0610 UT from the model at those 86 locations shown in Figure 2. One can see from Figure 6 that the model d*B*/d*t* values exhibit significantly large values at high latitudes due to auroral electrojet currents. However, the model-simulated d*B*/d*t* values below the auroral latitudes are smaller compared to the magnetometer observations shown in Figure 2. For example, the peak d*B*/d*t* values at Alibag and Tirunelveli are ∼8 and 43 nT/min in the model results compared to magnetometer observations of −25 and −136 nT/min, respectively. This difference between the model-computed d*B*/d*t* and magnetometer observations could be one of the limitations of the MHD model in capturing the magnetic field perturbations associated with PPEF and EEJ disturbances at the equatorial and low latitudes.

5. Conclusions

Equatorial GICs can be of similar magnitudes to that at high latitudes and are equally important. This study reveals that a sharp decrease in density at the front boundary of MC can cause large GICs at equatorial latitudes of the magnitudes that concern to the electric power systems under suitable conditions. Under the prevailing strong southward IMF Bz conditions (low Mach number), the variation of density controls the dayside reconnection rate and the convection electric field through the modulation of magnetosheath magnetic field. In such conditions, a sudden drop in the density, such as at the front boundary of MC, can lead to a sharp reduction in convection and dominance of shielding electric fields. The westward-shielding fields penetrate promptly to the low latitudes and the resultant SI^- will be amplified several times at the equator via the equatorial electrojet causing a large d*B*/d*t*. This study provides new insights into the equatorial GICs and the responsible mechanisms, which have direct applications in forecasting the GIC risk alerts to the power system operators.

Data Availability Statement

The magnetometer data of INTERMAGNET and WDC Kyoto University stations can be downloaded from https://www.intermagnet.org/data-donnee/download-eng.php and http://wdc.kugi.kyoto-u.ac.jp/caplot/index.html, respectively. The solar wind and SymH index data were obtained from NASA OMNI—Space Physics Data Facility (https://omniweb.gsfc.nasa.gov/form/omni_min.html). The magnetometer observations of Tirunelveli and Alibag are available from WDC Mumbai at http://wdciig.res.in/WebUI/MinData.aspx. The simulation results provided by the Community Coordinated Modeling Center (CCMC) at Goddard Space Flight Center through their public Runs on Request system are available at https://ccmc.gsfc.nasa.gov/results/viewrun.php?domain=GM&runnumber=Nilam_Bhosale_070721_1. The BATSRUS model tools developed at the University of Michigan's Center are available under the Space Weather Modeling Framework at https://clasp.engin.umich.edu/research/theory-computational-methods/swmf-downloadable-software/ and model runs can be carried out

through CCMC platform at https://ccmc.gsfc.nasa.gov/models/modelinfo.php?model=SWMF/BATS-R-US%20with%20RCM.

Acknowledgments
This work was supported by the Department of Science and Technology, Government of India.

References

Araki, T. (1977). Global structure of geomagnetic sudden commencements. *Planetary and Space Science*, *25*(4), 373–384. https://doi.org/10.1016/0032-0633(77)90053-8

Araki, T. (1994). A physical model of the geomagnetic sudden commencement. In M. J. Engebretson, K. Takahashi, & M. Scholer (Eds.), *Solar wind sources of magnetospheric ultra-low-frequency waves* (pp. 183–200). AGU.

Baker, D. N. (2002). How to cope with space weather. *Science*, *297*(5586), 1486–1487. https://doi.org/10.1126/science.1074956

Balan, N., Ebihara, Y., Skoug, R., Shiokawa, K., Batista, I. S., Tulasi Ram, S., et al. (2017). A scheme for forecasting severe space weather. *Journal of Geophysical Research: Space Physics*, *122*(3), 2824–2835. https://doi.org/10.1002/2016JA023853

Burlaga, L. F., Fitzenreiter, R., Lepping, R., Ogilvie, K., Szabo, A., Lazarus, A., et al. (1998). A magnetic cloud containing prominence material: January 1997. *Journal of Geophysical Research*, *103*(A1), 277–285. https://doi.org/10.1029/97ja02768

Burlaga, L. F., Klein, L., Sheeley, N. R., Michels, D. J., Howard, R. A., Koomen, M. J., et al. (1982). A magnetic cloud and a coronal mass ejection. *Geophysical Research Letters*, *9*(12), 1317–1320. https://doi.org/10.1029/gl009i012p01317

Burlaga, L. F., Sittler, E., Mariani, F., & Schwenn, R. (1981). Magnetic loop behind an interplanetary shock: Voyager, Helios and IMP 8 observations. *Journal of Geophysical Research*, *86*(A8), 6673. https://doi.org/10.1029/ja086ia08p06673

Carter, B. A., Yizengaw, E., Pradipta, R., Halford, A. J., Norman, R., & Zhang, K. (2015). Interplanetary shocks and the resulting geomagnetically induced currents at the equator. *Geophysical Research Letters*, *42*(16), 6554–6559. https://doi.org/10.1002/2015GL065060

Carter, B. A., Yizengaw, E., Pradipta, R., Weygand, J. M., Piersanti, M., Pulkkinen, A., et al. (2016). Geomagnetically induced currents around the world during the 17 March 2015 storm. *Journal of Geophysical Research: Space Physics*, *121*(10), 10496–10507. https://doi.org/10.1002/2016JA023344

Cliver, E. W., Ling, A. G., & Richardson, I. G. (2003). Coronal mass ejections, the tail of the solar wind magnetic field distribution, and 11 year cosmic-ray modulation at 1 AU. *The Astrophysical Journal*, *592*(1), 574–579. https://doi.org/10.1086/375616

Gaunt, C., & Coetzee, G. (2007). Transformer failures in regions incorrectly considered to have low GIC-risk. In *Power Tech, 2007 IEEE Lausanne* (pp. 807–812). IEEE. https://doi.org/10.1109/PCT.2007.4538419

Gopalswamy, N. (2003). Coronal mass ejections: Initiation and detection. *Advances in Space Research*, *31*(4), 869–881. https://doi.org/10.1016/S0273-1177(02)00888-8

Gopalswamy, N. (2006). Properties of interplanetary coronal mass ejections. *Space Science Reviews*, *124*(1–4), 145–168. https://doi.org/10.1007/s11214-006-9102-1

Gosling, J. T. (1996). Corotating and transient solar wind flows in three dimensions. *Annual Review of Astronomy and Astrophysics*, *34*(1), 35–73. https://doi.org/10.1146/annurev.astro.34.1.35

Haiducek, J. D., Welling, D. T., Ganushkina, N. Y., Morley, S. K., & Ozturk, D. S. (2017). SWMF global magnetosphere simulations of January 2005: Geomagnetic indices and cross-polar cap potential. *Space Weather*, *15*(12), 1567–1587. https://doi.org/10.1002/2017SW001695

Harel, M., Wolf, R. A., Reiff, P. H., Spiro, R. W., Burke, W. J., Rich, F. J., & Smiddy, M. (1981). Quantitative simulation of a magnetospheric substorm. 1. Model logic and overview. *Journal of Geophysical Research*, *86*(A4), 2217. https://doi.org/10.1029/ja086ia04p02217

Kane, R. P. (1974). Relation between the strength of the Sq current system and its focus position. *Proceedings of the Indian Academy of Sciences – Section A*, *80*(A80), 17–25. https://doi.org/10.1007/bf03046669

Kappenman, J. G. (2005). An overview of the impulsive geomagnetic field disturbances and power grid impacts associated with the violent Sun-Earth connection events of 29–31 October 2003 and a comparative evaluation with other contemporary storms. *Space Weather*, *3*(8), 08C01. https://doi.org/10.1029/2004SW000128

Kataoka, R., Fairfield, D. H., Sibeck, D. G., Rastätter, L., Fok, M.-C., Nagatsuma, T., & Ebihara, Y. (2005). Magnetosheath variations during the storm main phase on 20 November 2003: Evidence for solar wind density control of energy transfer to the magnetosphere. *Geophysical Research Letters*, *32*(21), L21108. https://doi.org/10.1029/2005GL024495

Kikuchi, T., Hashimoto, K. K., Kitamura, T. I., Tachihara, H., & Fejer, B. J. (2003). Equatorial counter electrojets during substorms. *Journal of Geophysical Research*, *108*(A11), 1406. https://doi.org/10.1029/2003JA009915

Kikuchi, T., Luhr, H., Kitamura, T., Saka, O., & Schlegel, K. (1996). Direct penetration of the polar electric fields to the equator during a DP 2 event as detected by the auroral and equatorial magnetometer chains and the EISCAT radar. *Journal of Geophysical Research*, *101*(A8), 17161–17173. https://doi.org/10.1029/96JA01299

Klein, L. W., & Burlaga, L. F. (1982). Interplanetary magnetic clouds at 1 AU. *Journal of Geophysical Research*, *87*(A2), 613–624. https://doi.org/10.1029/ja087ia02p00613

Kwagala, N. K., Hesse, M., Moretto, T., Tenfjord, P., Norgren, C., Tóth, G., et al. (2020). Validating the space weather modeling framework (SWMF) for applications in northern Europe. *Journal of Space Weather and Space Climate*, *10*, 33. https://doi.org/10.1051/swsc/2020034

Lepping, R. P., Burlaga, L. F., Szabo, A., Ogilvie, K. W., Mish, W. H., Vassiliadis, D., et al. (1997). The Wind magnetic cloud and events of October 18–20, 1995: Interplanetary properties and as triggers for geomagnetic activity. *Journal of Geophysical Research*, *102*(A7), 14049–14064. https://doi.org/10.1029/97ja00272

Lepping, R. P., Jones, J. A., & Burlaga, L. F. (1990). Magnetic field structure of interplanetary magnetic clouds at 1 AU. *Journal of Geophysical Research*, *95*(A8), 11957. https://doi.org/10.1029/ja095ia08p11957

Liemohn, M., Ganushkina, N. Y., De Zeeuw, D. L., Rastaetter, L., Kuznetsova, M., Welling, D. T., et al. (2018). Real-time SWMF at CCMC: Assessing the Dst output from continuous operational simulations. *Space Weather*, *16*(10), 1583–1603. https://doi.org/10.1029/2018SW001953

Lopez, R. E., Wiltberger, M., Hernandez, S., & Lyon, J. G. (2004). Solar wind density control of energy transfer to the magnetosphere. *Geophysical Research Letters*, *31*(8), L08804. https://doi.org/10.1029/2003GL018780

Morley, S. K., Welling, D. T., & Woodroffe, J. R. (2018). Perturbed input ensemble modeling with the space weather modeling framework. *Space Weather*, *16*(9), 1330–1347. https://doi.org/10.1029/2018SW002000

Nilam, B., Ram, S. T., Shiokawa, K., Balan, N., & Zhang, Q. (2020). The solar wind density control on the prompt penetration electric field and equatorial electrojet. *Journal of Geophysical Research: Space Physics*, *125*(9), e2020JA027869. https://doi.org/10.1029/2020JA027869

Nishida, A. (1968). Coherence of geomagnetic *DP* 2 fluctuations with interplanetary magnetic variations. *Journal of Geophysical Research*, *73*(17), 5549–5559. https://doi.org/10.1029/JA073i017p05549

Ober, D. M., Thomsen, M. F., & Maynard, N. C. (2002). Observations of bow shock and magnetopause crossings from geosynchronous orbit on 31 March 2001. *Journal of Geophysical Research*, *107*(A8), 1206. https://doi.org/10.1029/2001JA000284

Ober, D. M., Wilson, G. R., Burke, W. J., Maynard, N. C., & Siebert, K. D. (2007). Magnetohydrodynamic simulations of transient transpolar potential responses to solar wind density changes. *Journal of Geophysical Research*, *112*(A10), A10212. https://doi.org/10.1029/2006JA012169

Oliveira, D. M., Arel, D., Raeder, J., Zesta, E., Ngwira, C. M., Carter, B. A., et al. (2018). Geomagnetically induced currents caused by interplanetary shocks with different impact angles and speeds. *Space Weather*, *16*(6), 636–647. https://doi.org/10.1029/2018SW001880

Pulkkinen, A., Bernabeu, E., Eichner, J., Beggan, C., & Thomson, A. W. P. (2012). Generation of 100-year geomagnetically induced current scenarios. *Space Weather*, *10*(4), S04003. https://doi.org/10.1029/2011SW000750

Pulkkinen, A., Rasttter, L., Kuznetsova, M., Singer, H., Balch, C., Weimer, D., et al. (2013). Community-wide validation of geospace model ground magnetic field perturbation predictions to support model transition to operations. *Space Weather*, *11*(6), 369–385. https://doi.org/10.1002/swe.20056

Rastogi, R. G. (1977). Geomagnetic storms and electric fields in the equatorial ionosphere. *Nature*, *268*(5619), 422–424. https://doi.org/10.1038/268422a0

Reddy, C. A. (1989). The equatorial electrojet. *Pure and Applied Geophysics*, *131*(3), 485–508. https://doi.org/10.1007/BF00876841

Ridley, A. J., Gombosi, T. I., & DeZeeuw, D. L. (2004). Ionospheric control of the magnetosphere: Conductance. *Annales Geophysicae*, *22*(2), 567–584. https://doi.org/10.5194/angeo-22-567-2004

Ridley, A. J., & Liemohn, M. W. (2002). A model-derived storm time asymmetric ring current driven electric field description. *Journal of Geophysical Research*, *107*(A8). https://doi.org/10.1029/2001JA000051

Russell, C. T. (1976). On the occurrence of magnetopause crossings at 6.6 RE. *Geophysical Research Letters*, *3*(10), 593–595. https://doi.org/10.1029/gl003i010p00593

Sastri, J. H. (2002). Penetration electric fields at the nightside dip equator associated with the main impulse of the storm sudden commencement of 8 July 1991. *Journal of Geophysical Research*, *107*(A12), 1448. https://doi.org/10.1029/2002JA009453

Sastri, J. H., Huang, Y. N., Shibata, T., & Okuzawa, T. (1995). Response of equatorial-low latitude ionosphere to sudden expansion of magnetosphere. *Geophysical Research Letters*, *22*(19), 1649–2652. https://doi.org/10.1029/95gl02669

Senior, C., & Blanc, M. (1984). On the control of magnetospheric convection by the spatial distribution of ionospheric conductivities. *Journal of Geophysical Research*, *89*(A1), 261–284. https://doi.org/10.1029/JA089iA01p00261

Takeuchi, T., Araki, T., Viljanen, A., & Watermann, J. (2002). Geomagnetic negative sudden impulses: Interplanetary causes and polarization distribution. *Journal of Geophysical Research*, *107*(A7), 1096. https://doi.org/10.1029/2001JA900152

Toffoletto, F., Sazykin, S., Spiro, R., & Wolf, R. (2003). Inner magnetospheric modeling with the rice convection model. *Space Science Reviews*, *107*(1/2), 175–196. https://doi.org/10.1007/978-94-007-1069-6_19

Tóth, G., Sokolov, I. V., Gombosi, T. I., Chesney, D. R., Clauer, C. R., De Zeeuw, D. L., et al. (2005). Space weather modeling framework: A new tool for the space science community. *Journal of Geophysical Research*, *110*(A12), A12226. https://doi.org/10.1029/2005JA011126

Tulasi Ram, S., Nilam, B., Balan, N., Zhang, Q., Shiokawa, K., Chakrabarty, D., et al. (2019). Three different episodes of prompt equatorial electric field perturbations under steady southward IMF Bz during St. Patrick's Day storm. *Journal of Geophysical Research: Space Physics*, *124*(12), 10428–10443. https://doi.org/10.1029/2019JA027069

Viljanen, A. (1998). Relation of geomagnetically induced currents and local geomagnetic variations. *IEEE Transactions on Power Delivery*, *13*(4), 1285–1290. https://doi.org/10.1109/61.714497

Wang, Y. M., Ye, P. Z., & Wang, S. (2003). Multiple magnetic clouds: Several examples during March–April 2001. *Journal of Geophysical Research*, *108*(A10), 1370. https://doi.org/10.1029/2003JA009850

Yu, Y., & Ridley, A. J. (2008). Validation of the space weather modelling framework using ground-based magnetometers. *Space Weather*, *6*(5), S05002. https://doi.org/10.1029/2007SW000345